SOLID STATE FLUX MONITOR DEVELOPMENT, FABRICATION, AND TESTING

Subtask 2.1 of

INTERNATIONAL NUCLEAR ENERGY RESEARCH INITIATIVE

Between
United States of America and Republic of Korea

Project 2002-020-K

Development Of Enhanced Reactor Operation Strategy Through Improved Sensing And Control At Nuclear Power Plants

David E. Holcomb—Oak Ridge National Laboratory
Byung-Soo Moon—Korean Atomic Energy Research Institute
Don W. Miller & Joseph W. Talnagi—The Ohio State University

Final Project Report

February 2005

This Page Intentionally Left Blank

Table of Contents

Table of Figures

Table of Tables

Table of Acronyms

AlN ---------- Aluminum Nitride
a.u. ---------- Arbitrary Units
CIC ---------- Compensated Ion Chamber
CIF ---------- Central Irradiation Facility
CNS ---------- Cold Neutron Source
cps ---------- counts per second
CTE ---------- Coefficient of Thermal Expansion
DBC ---------- Direct Bonded Copper
EMI ---------- Electro-Magnetic Interference
KAERI ---------- Korean Atomic Energy Research Institute
HANARO ---------- High-Flux Advanced Neutron Application Reactor
LPRM ---------- local power range monitoring
LWR ---------- Light Water Reactor
MIMS ---------- Mineral Insulated Metal Sheathed
NPP ---------- Nuclear Power Plant
nv ---------- Neutron density times Velocity; $\frac{neutrons}{cm^2 - s}$
ORNL ---------- Oak Ridge National Laboratory
OSU ---------- The Ohio State University
OSURR ---------- The Ohio State University Research Reactor
PNF ---------- Pohang Neutron Facility
SPND ---------- Self Powered Neutron Detector
SSFM ---------- Solid State Flux Monitor

This Page Intentionally Left Blank

ALUMINUM NITRIDE SOLID STATE FLUX MONITOR DESIGN, FABRICATION, AND DEMONSTRATION

1 Project Summary

The objective of this project was to design, fabricate, and demonstrate a solid-state flux monitor (SSFM) for use in-core, at power in nuclear power plants (NPPs). A novel detector, based upon the $^{14}N(n,p)^{14}C$ reaction in aluminum nitride (AlN), was conceived, developed, and demonstrated. The sensor essentially consists of a polycrystalline aluminum nitride ceramic compact configured as a flux sensitive resistor. Neutron capture in the ^{14}N produces free electrical carriers as the resultant energetic daughter particles slow down within the sensor. The ceramic compact is a small (3 mm x 3 mm x ~500 μm thick) high electrical resistance chip with direct bonded copper contacts (1.5 mm in diameter) on opposing sides, resembling a parallel plate capacitor. Bias voltage is applied to sweep the free carriers through the compact resulting in a current proportional to the ionizing dose deposited in the sensor body. The sensor's performance is similar to that expected theoretically. The device sensitivity is low enough to endure in-core, at-power conditions yet high enough to readily observe power level changes. The current development state of the sensors does have remaining unknown and undesirable performance characteristics and further research is recommended. While the sensor is designed to function in-core, at power for years, this has not yet been demonstrated. Consequently, the device's long-term survival remains unknown. The detector is intended to function at both light water reactor characteristic temperatures and the higher temperatures of Generation IV reactors. For current generation sensors at temperatures significantly above those of light water reactors, the detector leakage current becomes a significant fraction of the measured signal. Also, a more thorough study of electric field driven impurity migration within the detector is recommended, as the sensing elements appear to polarize with time at voltage.

This project was divided into two coupled subtasks. The first subtask, design and fabrication of prototype flux monitors, was led by the Oak Ridge National Laboratory (ORNL) with the Korean Atomic Energy Research Institute (KAERI) providing support and being responsible for the device packaging. The second subtask, performance testing, was jointly performed by KAERI and The Ohio State University (OSU).

Following initial performance requirements analysis, ORNL selected AlN as the candidate detector material, and polycrystalline, sintered compacts as the physical form for the sensor body. A series of progressively more refined prototype sensors were fabricated and their performance evaluated. Adhering the electrical contacts onto the AlN substrate and then joining the wires to the devices without cracking the AlN and in a rugged enough fashion to endure both manipulation and temperature cycling proved to be the most technically challenging aspect of the device fabrication. Much of the device testing was performed with bare sensors. Sensors for in-core testing were encapsulated into Inconel 600™ alloy shells with MgO powder insulation. The sensor electrical leads were brazed to the conductors of mineral insulated metal-sheathed (MIMS) cable and the sensor shell was seal welded to the cable sheath. Detector neutron performance was demonstrated at HANARO (at a beam port and within core), the Ohio State University Research Reactor (OSURR), the Pohang Neutron Facility (PNS), and the Ohio State

subcritical assembly. Gamma ray device response was measured by KAERI using gamma sources ranging from a 18.5 kBq (500 nCi) to 7.5 PBq (200 kCi) ^{60}Co.

2 Background

2.1 Project Rationale

Local power-range flux monitoring is desirable for any commercial power reactor. Measuring the local neutron flux at-power is important to observe phenomena ranging from boric acid plate out to axial power offset anomalies. Local power range monitoring (LPRM) is also important to the design of gas-cooled, graphite-moderated power reactor cores as the local power peaking restricts the core power density. Measuring, as opposed to calculating, the local power peaking is particularly important for gas-cooled, graphite-moderated reactors because of the sharp (and consequently difficult to calculate) flux peaking at the fuel to graphite boundary and the manufacturing and assembly variability of the components.

A common feature of Generation IV reactors is their higher operating temperatures. A technical objective of the new AlN SSFM is to increase the available temperature for LPRM as compared to miniature fission chambers while not incurring the delays or signal-to-noise ratio restrictions of (self-powered neutron detectors) SPNDs.

Solid phase materials have not generally been considered as candidates for transducers in-core because many properties of semiconducting solids are much more susceptible to radiation damage than gases. Single crystal based detectors would only survive transiently in a nuclear reactor core as the intense radiation field would rapidly destroy the long-range crystalline order which is important to charge transport properties. Highly polycrystalline, refractory solids, in contrast, are (in terms of electronic transport properties) much more radiation tolerant. Small grain size, refractory polycrystalline solids begin in a disordered state on a long-range scale and so are not vulnerable to radiation induced disordering. In terms of short-range order, refractory ceramics are very chemically stable. Consequently, both ionizing and displacement doses are highly likely to result in functionally identical material.

Boron-10 containing solids were first investigated as neutron flux sensitive resistors more than thirty years ago.[1] However, almost none of the significant parameters required to employ such devices as reliable flux monitors in nuclear power plants have previously been determined. Prior efforts at semiconductor based neutron detection have also generally focused on maximizing device sensitivity whereas restricting the neutron sensitivity to minimize both the atomic burn-up as well as the device self-heating is an important design consideration for an in-core, at-power neutron sensor. Materials containing significant amounts of ^{10}B are inappropriate for deployment in core for flux measurement as they locally depress the flux, heat rapidly and atomically burn-up significantly in short periods of time. The ^{14}N(n,p)^{14}C reaction has previously been employed for detectors in high flux situations (beam line monitors for neutron scattering experiments) where its significant but low neutron capture cross section is advantageous.[2]

2.2 Competing LPRM Technologies

2.2.1 Miniature Fission Chambers

Miniature fission chambers are currently used in-core in water-moderated reactors for local flux measurements.[3] They respond to a combination of neutrons and gamma rays. A noteworthy, innovative micro-fission chamber is currently under development for in-core deployment by Kansas State University.[4] These detectors are scaled down versions of conventional fission chambers that are fabricated using microelectromechanical device techniques.

The expense and complication of disposal of spent fission chambers both due to the highly radioactive fission products and the residual fissionable material in the exhausted detector is the single largest limitation to their use. Further, traditional miniature fission chambers require significant technological change to extend to higher temperature ranges (above that in water cooled reactors) due both to conductive deposits accumulating on their insulators and failures of the interior electrical joints. Also, gas phase neutron detector instrumentation becomes progressively more difficult to employ as temperatures increase due to the requirement to seal the gas volume. The seals are more technologically challenging at higher temperatures both due to the coefficient of thermal expansion (CTE) mismatch between conductors and insulators as well as the increasing gas pressure with temperature.

2.2.2 Self Powered Neutron Detectors (SPNDs)

While extending SPNDs to higher temperature appears easier than gas-filled detectors due to their lack of gas sealing requirements and the high-temperature tolerance of commonly used vanadium and rhodium emitters, their low signal strength and delayed response makes them undesirable for many applications. SPNDs have low enough sensitivity (5×10^{-23} A/nv$_{th}$/cm for a Vanadium wire) so as to be sensitive to radiation-induced conductivity in the cables requiring a dummy unconnected compensation lead in the cabling. As small signal devices SPNDs are also sensitive to electromagnetic pick-up.

2.2.3 Silicon Carbide Diodes

The largest limitation to the use of silicon carbide diodes in-core, at power is their comparatively high radiation sensitivity. SiC based neutron detectors have only been shown to operate in fast neutron (1 MeV equivalent) fluences of up to 10^{17} neutrons/cm^2.[5] SiC based neutron detectors are just emerging from the experimental stage. A recent overview of their operation has been given by Ruddy et al.[6] SiC Schottky diode based neutron detectors with a lithium fluoride converter layer above the diode feature very high gamma rejection capabilities due to their thin active depth and the low linear energy transfer of the energetic electrons resulting from gamma interaction. SiC based neutron detectors also are capable of very high-speed operation (GHz bandwidth) allowing for pulse mode operation through power range. SiC has the potential for at least 800 °C operation and it has been shown that damage annealing takes place in the 800-1000 °C range. However, operation has only been demonstrated to ~350 °C.

An additional concern for SiC-based neutron detectors is that only a small fraction of the total neutron capture reaction kinetic energy is actually deposited within the detector

sensitive volume, and the devices are not operated in an avalanche mode, so the signal pulses are quite small. The pulses also tend to have sharp rise and fall times due to the small device capacitance. The combined small size and high frequency content of the neutron induced pulses means that the first stage preamplifiers for these devices need to be located relatively close to the detector. The cable isolation and grounding quality requirements are more stringent for these detectors than competing types.

3 Design and Operating Principles

The central idea of the solid-state flux monitor is to use a group III nitride as a flux sensitive resistor. Simply put a piece of group III nitride material has electrical contacts made to its surface, voltage is applied to the contacts, it is placed into a neutron field, and the measured electrical current is the signal. Figure 1 illustrates the situation.

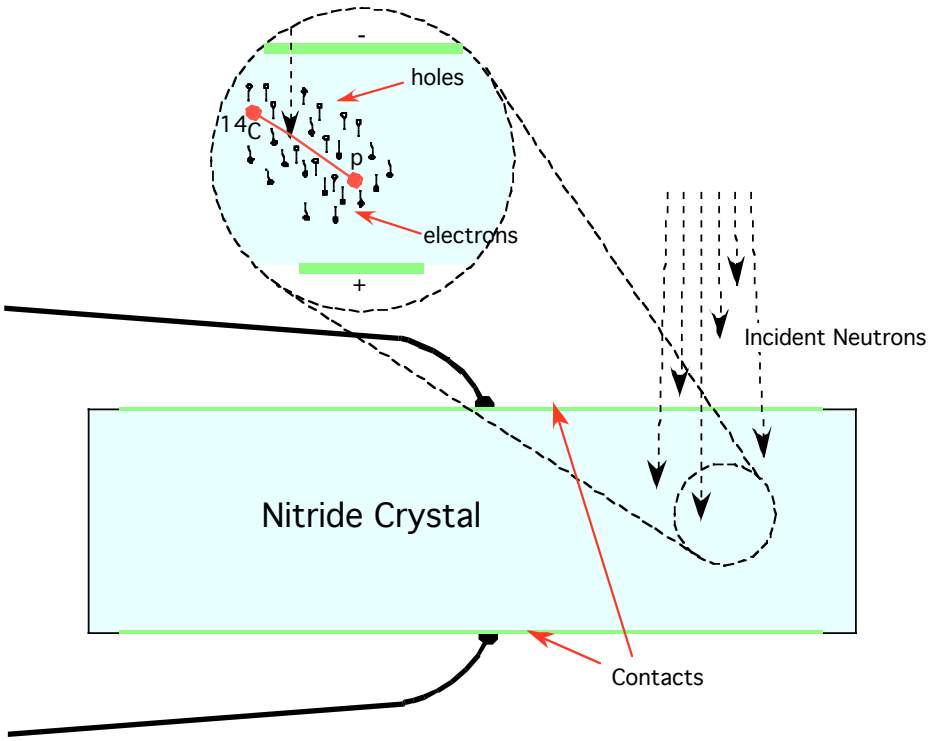

Figure 1—Conceptual layout and physical arrangement of a solid-state flux monitor

3.1 Required Sensor Material Properties

In order to function as a neutron flux sensitive resistor a material must possess particular material properties. First the material must have high electrical resistance. The sensor signal consists of the neutron-induced current. Non-neutron induced current is a noise signal, so the sensor resistance must be large enough to allow the extraction of the neutron induced current from all other electrical currents. One of the electrical currents of particular concern is thermally induced current. Since Generation IV nuclear reactor core operational temperatures are significantly higher than water moderated reactors, the sensor material must continue to exhibit high electrical resistances at as high as possible a temperature.

Another electrical property the sensor must exhibit is a high free carrier mobility lifetime product. The first step in the process by which neutrons generate an electrical current in the sensor is through creating free-carriers via the slowing down of the energetic daughter particles resulting from a nuclear reaction. These free carriers (electron-hole pairs) must be free to move appreciably to serve as a current. In many wide band-gap materials such as silica or sapphire the free-carrier lifetime is less than a picosecond, so the carriers do not move appreciably under an applied voltage and thus not produce a measurable current. All of the group III nitrides, to the extent that their properties are known, exhibit high carrier mobilities. The properties of the group III nitrides are reviewed in the recent compilation "Properties of the Group III Nitrides."[7]

A further electrical property that the sensor material must exhibit is good electrical field penetration. In many materials one of the constituent atoms or an atomic impurity is mobile with applied electric field. In this case, the mobile species moves toward the electrode of the opposite polarity and the rearrangement of the charge within the material neutralizes the field within the sensor. Essentially the material functions as an electrolytic capacitor with near zero internal field away from the region immediately adjacent to the electrodes. Note that the figure-of-merit most commonly used when comparing the electrical properties of various detector materials is the schubweg, which is the product of the carrier mobility, the electric field, and the carrier lifetime.

Another required property for the flux sensitive resistor material is that it must have a significant neutron interaction probability. Nitrogen-14, which composes 99.6% of naturally occurring nitrogen, has a significant (1.769 b at 25.3 meV) inverse neutron velocity proportional energetic proton production cross-section. This means that all of the group III nitrides have a significant neutron interaction cross-section. Furthermore the Boron-10 isotope of boron nitride has a very high neutron induced alpha particle production cross-section. Boron nitride is therefore interesting for situations requiring higher sensitivity. Figure 2 shows the neutron induced charged particle production cross sections for ^{14}N, ^{10}B and ^{27}Al.

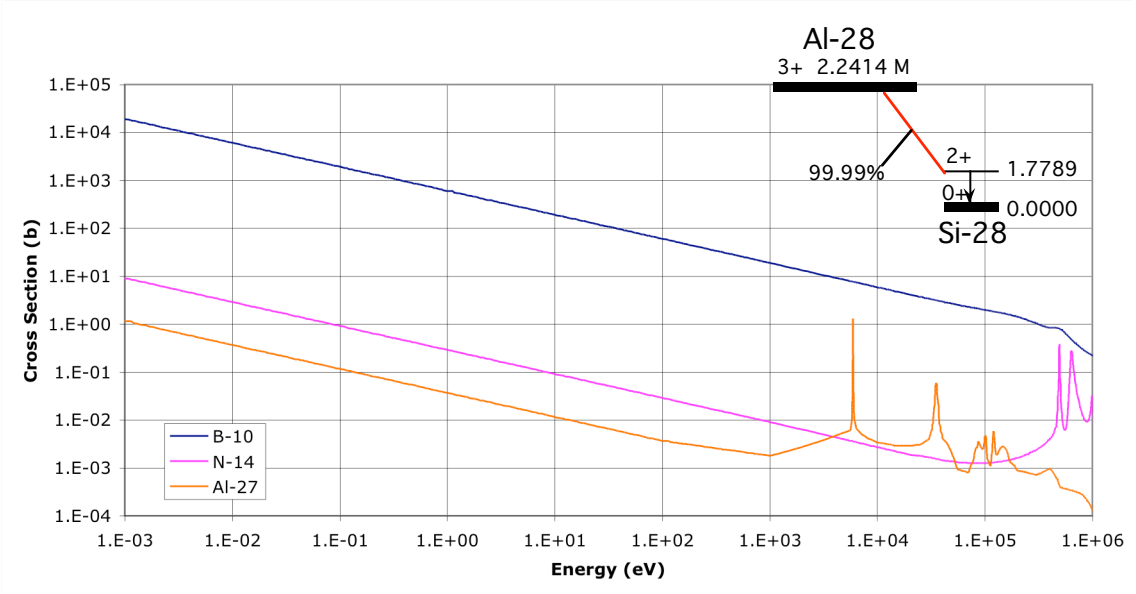

Figure 2—Nitrogen-14, Boron-10, and Aluminum-27 Neutron Induced Charged Particle Production Cross Sections

The neutron interaction within the sensor material must yield energetic charged particles to generate electron-hole pairs as the energetic charged particles slow down in the material. Both ^{10}B and ^{14}N have neutron capture reactions that yield energetic charged daughter particles as shown in equations (1) and (2).

$$^{14}N + {}^{1}n \rightarrow {}^{14}C + {}^{1}p \quad \begin{pmatrix} E_C = 42\,keV \\ E_p = 585\,keV \end{pmatrix} \tag{1}$$

$$^{10}B + {}^{1}n \rightarrow \begin{cases} {}^{7}Li + {}^{2}\alpha \quad (6\%) \\ {}^{7}Li + {}^{2}\alpha + \gamma \quad \begin{pmatrix} E_\gamma = 480\,keV \\ 94\% \leftrightarrow E_{Li} = 840\,keV \\ E_\alpha = 1.47\,MeV \end{pmatrix} \end{cases} \tag{2}$$

Other desirable properties for the sensor material include: mechanical robustness, invariance in response with flux and dose, high chemical inertness, and a reasonable fabrication route. Both aluminum nitride and boron nitride appear to possess all of the required properties to function as neutron flux monitors. Aluminum nitride, however, appears to be more suitable for in-core, at power deployments. Boron nitride will have a significantly higher sensitivity, but will suffer from more rapid burn-up as well as very high thermal loading under high fluxes.

3.2 Estimation of Device Response

The basic device response estimation involves applying standard physical models for each of the physical processes involved in the detection process to yield an estimate of the electrical current produced per unit neutron flux. The electrical resistance of high purity aluminum nitride remains very high (in terms of the thermal leakage current compared to the expected signal current) for temperatures up well above water reactor coolant temperatures.

In the case of AlN, the neutron interaction has a Q-value of 627 keV. Aluminum nitride has a band-gap of 6.28 eV. The rule-of-thumb is that a free carrier is produced for every three-fold of the band-gap deposited into the material by an energetic electron. Protons, because of both their greater ionization density along the slowing down track as well as the increased fractional expenditure of energy in atomic rearrangement, are generally considered to be roughly one-third as efficient in generating free carriers as electrons. Roughly speaking, therefore, each neutron interaction within aluminum nitride can be expected to generate 10,000 free carriers. For a neutron flux of 10^{14} /cm^2-s, a 1 mm x 1 mm x 1 micron piece of aluminum nitride with a density of 3.23 g/cm^3 would be expected to generate 8.7×10^{10} e$^-$/s. Provided that these generated carriers move readily

across the sample, which appears likely due to the high electron mobility (~100 cm^2/V-s), this would produce a current of 3.5 μA for a 250 μm thick sample.

The annual burn-up at power for such a device would be roughly six parts per thousand. It is not expected that the device will have a significant radiation damage response because the physical form that is originally used is a disorganized polycrystalline solid. This is very likely the same structure that will reform under intense irradiation.

One potential concern about this device is that the intense gamma flux within the reactor will also produce a response that may be of the same magnitude as the neutron response. While in general the gamma flux at power in a nuclear reactor core is itself considered a measure of overall reactor power and hence may not be considered parasitic, it may be necessary to compensate for the gamma response of the device. This is technologically possible in much the same fashion as in a compensated ion chamber. Nitrogen-15 does not possess the thermal neutron absorption cross section of ^{14}N. Hence an otherwise identical device composed of ^{15}N based aluminum nitride would be expected to respond just as a ^{14}N aluminum nitride sensor, but without the low-energy neutron sensitivity. Therefore subtracting the currents from the two devices would yield the sensor current due to the thermal neutron flux. The only caveat to this technique is that isotopically separated aluminum nitride is not currently a commercial product and would have to be produced specifically for the sensor. While this is technologically feasible, it is cost prohibitive until the other performance aspects of the sensor have been demonstrated experimentally.

4 Fabrication and Packaging

4.1 Transducer Composition and Properties

The sensor body is formed from sintered aluminum nitride powder with a small amount of yttrium oxide added as a binder and oxygen getter that is cast and fired into sheets. The general properties of aluminum nitride are available on an electronic archive of semiconductor material properties.[8] Two different sources of supply for AlN pieces were used over the course of the project. First generation prototypes were 250 μm thick AlN pieces, polished on both sides, which were fabricated by Valley Design Corporation.[9] Later the transducer bodies were obtained in sheet form (381 μm and 635 μm thick) from Curamik® Electronics Inc.[10] (Toshiba Corp. manufactured substrate.) The AlN sheets were laser scribed and then mechanically broken into 3 mm x 3 mm squares. Figure 3a shows a sheet of AlN that has been scribed and had electrical contacts deposited (also by Curamik®). Figure 3b shows a close-up of a portion of the sheet showing the scribe lines and the gold-coated contact pads.

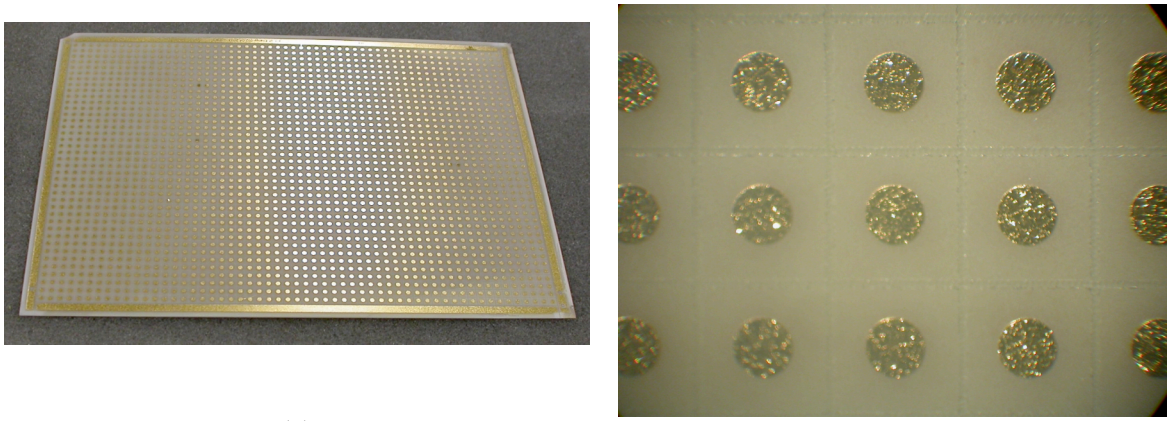

(a) (b)

Figure 3—(a) Sheet of AlN With Electrical Contact Pads and (b) Close-up of AlN Sheet Showing Scribe Lines and Electrical Contact Pads

4.2 Electrical Pad Deposition Technology

Forming electrical contacts on the AlN substrate that adhered well and tolerated thermal cycling consumed significant effort. Several different high-temperature metallization techniques were explored—notably including an alloy containing a small percentage of beryllium that proved too administratively difficult to use. A multi-layer brazing technique (600 μm titanium electron beam evaporated onto substrate at 300 °C[11] followed by a precious metal alloy braze for wire connection) was next developed and employed for the first generation of SSFM prototypes. This technique, however, was later supplanted by a direct bonded copper electrical contact pad deposition technique because of its much easier implementation, lower residual stress on the AlN substrate, and ease of integration with ultrasonic wire bonding. Direct bonded copper (DBC) contacting technology for metallizing aluminum nitride ceramic surfaces has been developed over the past decade in support of the semiconductor industry.[12] The direct copper bonding process starts with applying a copper sheet of the desired thickness to the surface of the aluminum nitride ceramic. A liquid shell is then formed around the copper sheet by heating under a reducing atmosphere resulting in a copper-oxygen eutectic melt on the surface of the aluminum nitride that wets and bonds to the ceramic. Patterning of the resultant copper layer is accomplished through standard semiconductor mask and etching techniques. To limit copper oxidation and ease wire attachment nickel and gold overlayers (a few microns thick) were applied over the copper (127 microns thick) contact spots. Copper electrical contact pads, 1.5 mm in diameter, were directly bonded to opposite sides of the chip. The transducer is shown in conceptual diagram form in Figure 4.

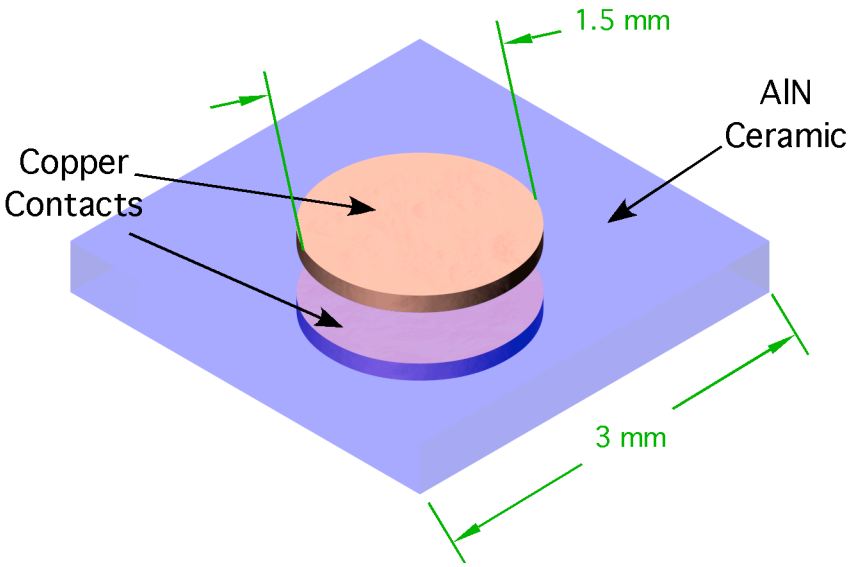

Figure 4—Conceptual Diagram of AlN Ceramic Compact With Electrical Contact Pads

4.3 Wire Connection Technology

Several different techniques were explored for joining wires to the metallized AlN substrate. The CTE mismatch between the AlN and most braze alloys resulted in cracking the substrate. A precious metal brazing technique (81.5% Au, 16.5% Cu, 2% Ni) employing Ni-10%Cr wire did provide effective bonds, but was difficult to implement on both sides of the substrate simultaneously and required considerable effort for each joint. Laser welding of refractory alloy wire (Nb-1%Zr) to the DBC spot was generally successful, but was difficult to replicate for multiple pieces and often resulted in a bond that could be relatively easily pulled off the surface.

Ultrasonic wire bonding of 127 µm diameter, soft copper wire proved a successful technique resulting in mechanical contacts that endured significant manipulation. Ultrasonic wire bonding is the most common technique employed in semiconductor manufacturing for joining wires that will experience higher temperatures. Ultrasonic wire bonding uses a combination of pressure and ultrasonic heating of the wire and substrate to create a joint and can rapidly be performed in air at room temperature. Figure 5 shows the final generation prototype transducer pieces employing a 381 µm thick AlN substrate with 127 µm thick copper contact pads overcoated with thin layers of nickel and gold with 127 µm diameter soft copper leads ultrasonically bonded to the electrical contact pads.

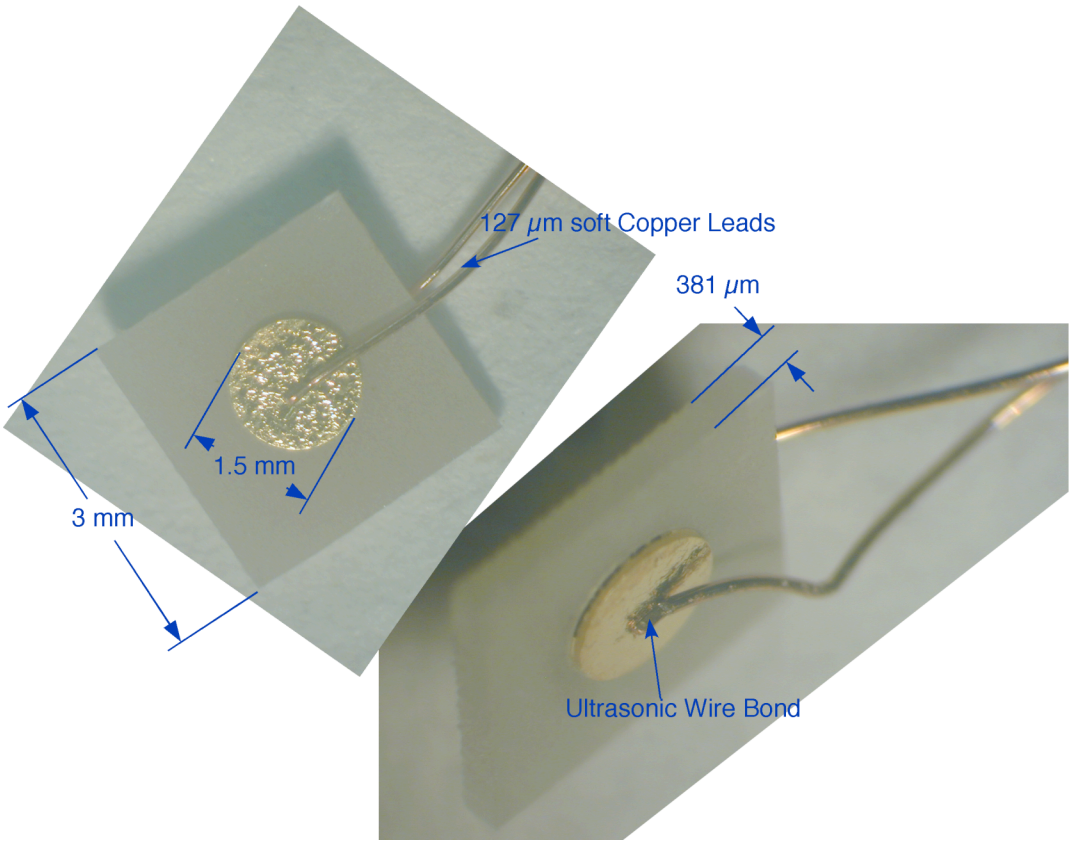

Figure 5—Bare Final Generation Prototype SSFMs Using Ultrasonic Wire Bonding

4.4 Protective Shell and MIMS Cable

In order to deploy the sensors in more aggressive environments, the bare devices needed to be encapsulated within a protective housing. Since the SSFMs are small signal devices, the housing is required to provide EMI shielding and physical isolation from the environment in addition to mechanical protection. The sensors leads were threaded onto a short piece dual bore ceramic tubing (thermocouple bead) and placed within a 1 cm OD Inconel™-600 sheath that was then backfilled with MgO powder. The leads were then brazed to a two-conductor 16 m long piece of MIMS cable from Thermocoax. Woojin Inc performed the encapsulation. A diagram of the sensor connection is shown as Figure 6.

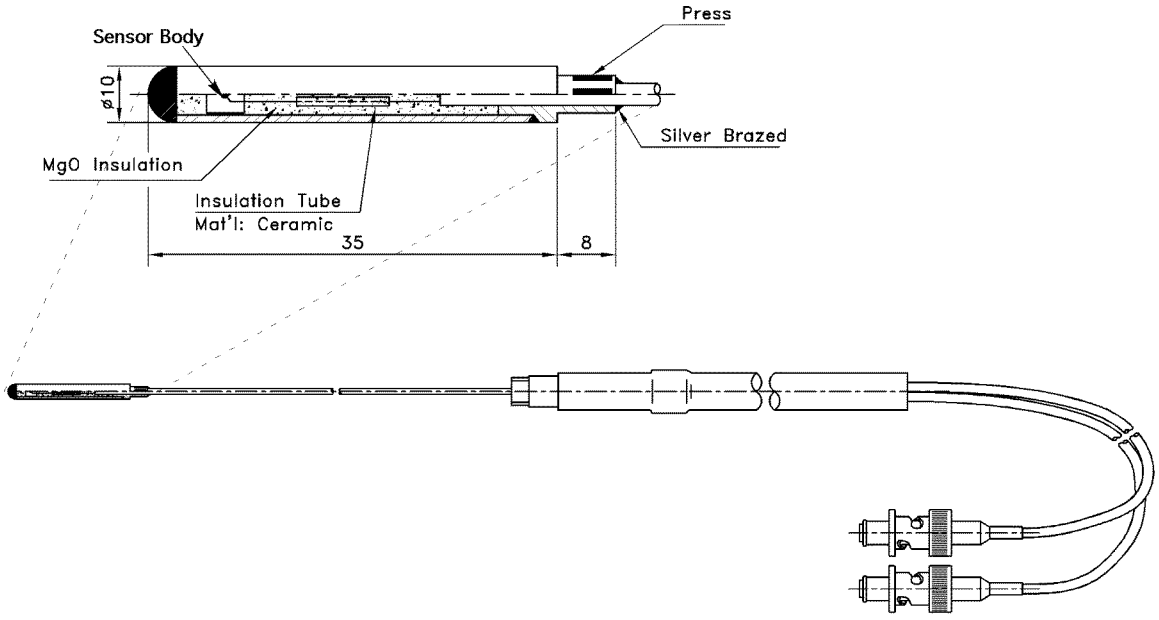

Figure 6—Diagram of Sensor Encapsulation

The measured resistance of the sensor after encapsulation was above 50 TΩ. The leakage current with 1000 V applied was about 20 pA with about 6 pA of fluctuation. The cable properties of this configuration restricted the applied voltage to < 1000 V. A photograph of the encapsulated sensor is shown as Figure 7.

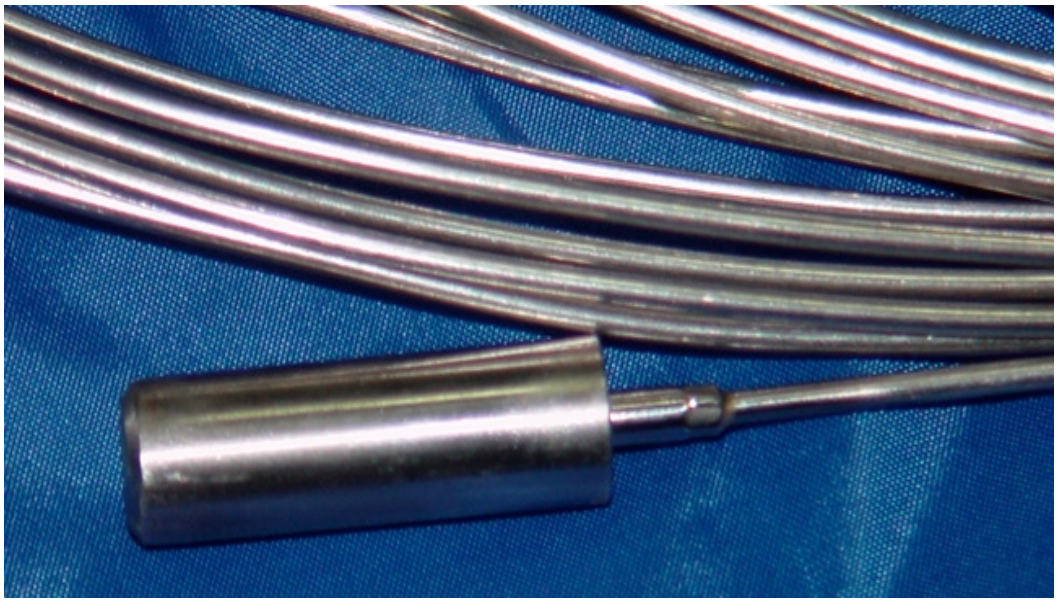

Figure 7—Encapsulated SSFM

The MIMS cable was later changed to a dual single conductor cable arrangement to allow higher voltages to be applied to the sensor. The relevant properties of MIMS cable employed are shown in Table 1. An additional advantage of the dual single conductor cable is the reduction in the sensitivity of the measurement to ionizing radiation produced current in the cable by reducing the field gradient across the insulation. While alumina

and magnesia are good insulators, in powder form they too yield a transient current under electric fields when subjected to ionizing radiation. If the SSFM is deployed in situations where the cable is exposed to a significant dose, it will be necessary to include a guard conductor (tri-axial configuration) in the cable to remove the cable contribution to the measured signal.

Table 1—Thermocoax Cable Properties

	Dual Conductor Cable	Single Conductor Model 1 II 30 AI
Sheath Material	Inconel™-600	Inconel™-600
Conductor	Inconel™-600	Inconel™-600
Insulator	99.6% alumina	99.6% alumina
Insulation Resistance [Ω-m]	10^{13} at 300 K	10^{13} at 300 K
Capacitance [pF/m]	280	280
Resistance [Ω/m]	11	3
Breakdown Voltage [V]	> 800V	> 1500 V
OD [mm]	2±0.03	3±0.03
Sheath Thickness [mm]	0.32±0.05	0.5±0.07
Conductor Diameter [mm]	0.32±0.05	0.7±0.07

4.5 Laboratory Mounting Configurations

Many of the laboratory measurements employed bare sensors with mechanically constrained leads. Figure 8a shows OSU's low-flux test mount for use within their sub-critical pile. Figure 8b shows OSU's mounting of the SSFM for electrical resistance versus temperature testing (note that the measurements were made with furnace power switched off).

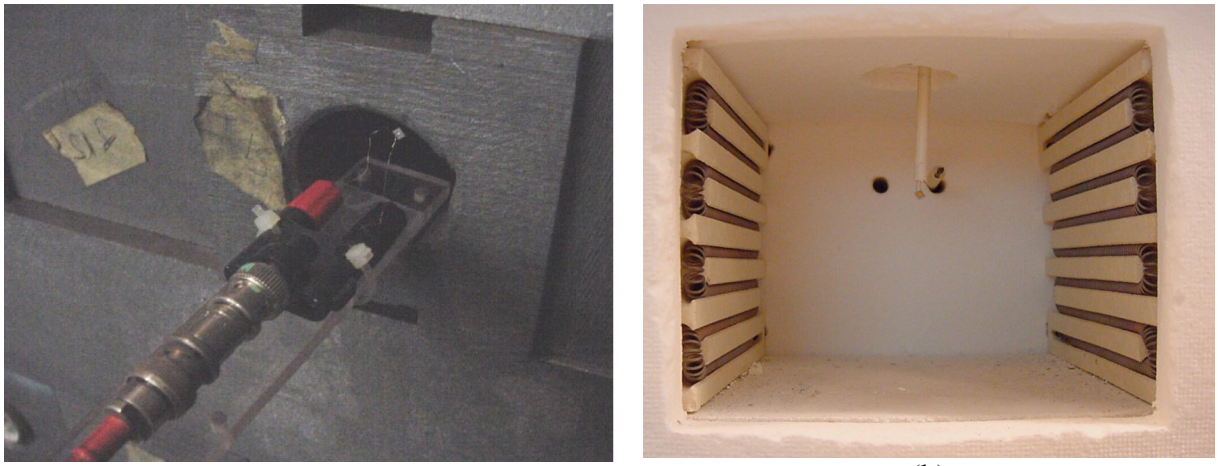

(a) (b)

Figure 8—(a) SSFM Mounting For Neutron Measurements at the OSU Subcritical Pile, and (b) SSFM Mounting Within Furnace at OSU

KAERI mounted the sensors within aluminum (gamma testing) or polyethylene (neutron testing) capsules. The capsules were mechanical mounts that served to keep the sensors

clean and mechanically supported, and to prevent them vibrating. Figure 9 shows two views of a mounted sensor.

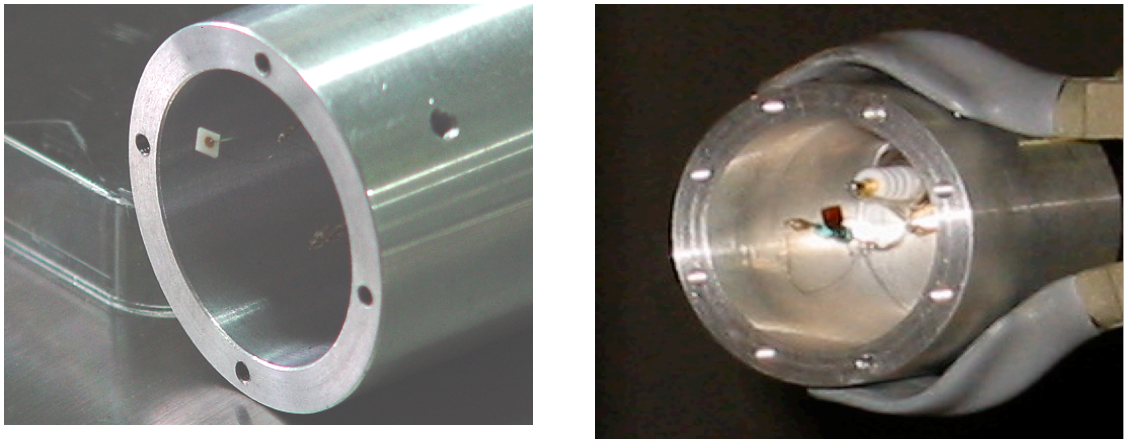

Figure 9—Two Views Of KAERI Aluminum Mounting Capsule With One End Opened

5 Device Testing And Performance

Essentially, the SSFM measures the total ionizing dose deposited within the sensor body. In a reactor core at power, the total ionizing dose is a combination of the dose due to gamma rays, that due to fast neutron collisions, and that due to lower energy neutron capture reactions. Since the gamma rays and the neutrons arise from fissions, both are useful for determining the reactor power. The response of the SSFMs to both pure gamma and almost pure neutron fields was also measured as part of characterizing the device performance. Both the thermal and intrinsic leakage currents of the device and packaging have also been characterized, as they constitute the principal error current leakage paths.

5.1 Non-Nuclear Device Characterization

Since the sensor functions as a dose sensitive resistor, the primary non-nuclear characterization was measurement of device leakage current both at room temperature and as a function of temperature. Also since the device has very high impedance and operates at relatively high voltages (>1000 V) it is important to prevent surface leakage currents. This means that the sensor's surface must be clean. The devices were repeatedly cleaned with organic solvents (2-Propanol and/or acetone) in ultrasonic cleaners and were further vacuum baked and coated with an epoxy resin for KAERI's measurements. Note that the sensors are particularly sensitive to humidity and require encapsulation for accurate resistance measurement in air. KAERI's room temperature measurements using a 635 μm thick sensor body indicate that the sensor has a resistance of ~10^{15} Ω.

Since the device is a very high impedance polycrystalline solid including a small binder phase, the electrical conduction mechanisms within it are a complex combination of conduction along the surface of the grains, field driven impurity and imperfection charge hopping through the individual crystals, field driven surface charge hopping, and charge trapping and release at the material interfaces. This means that the measured current,

while quite small, has a noise component that resembles the current pulses induced by individual radiation particle interactions. Further, to some extent, charged impurities within the crystal will be mobile within the material matrix. Over time they will move under the externally applied field and mask its penetration into the material. The extent to which this occurs depends on the material properties and the impurities and is a function of both temperature and the charged impurity radiolytic liberation occurring at high dose. A plot of the leakage current of a 635 µm thick AlN SSFM under 1000 V bias is shown as Figure 10.

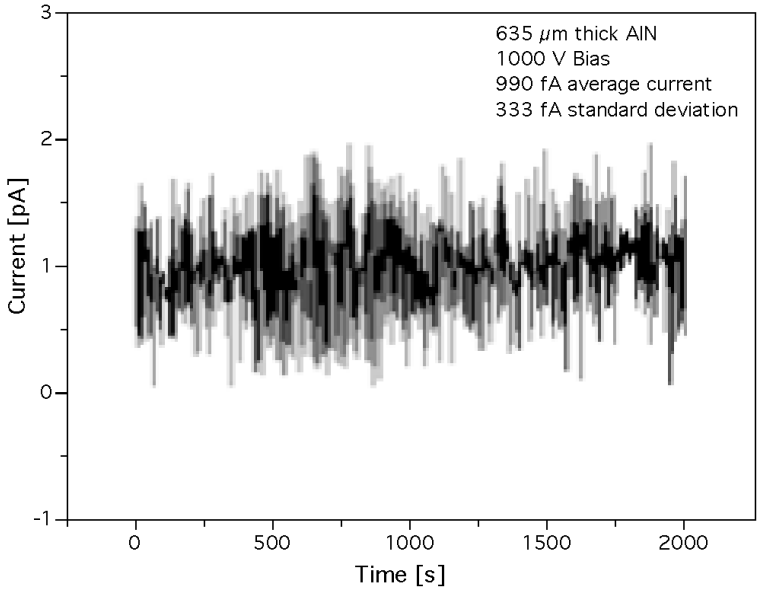

Figure 10—SSFM Leakage Current Variation Over Time

A plot of the measured sensor resistivity versus temperature is shown as Figure 11. The OSU and ORNL measured data agree well. The outlying data is from published data for a slightly different material; bulk, low-oxygen polycrystalline AlN.[13] The measurements demonstrate that the SSFM resistivity decreases logarithmically with temperature. The current SSFM configurations produce a few microamps of signal for power range in-core flux levels. This means that to restrict that thermal leakage current to less than 1% of the measured signal for a 381 µm thick sensor operating at 1000 V ~10^9 Ω-cm of resistivity is required. This limits non-thermally compensated operation to < 750 K. At 1000 K the sensor will exhibit a ~20% power range thermal leakage offset.

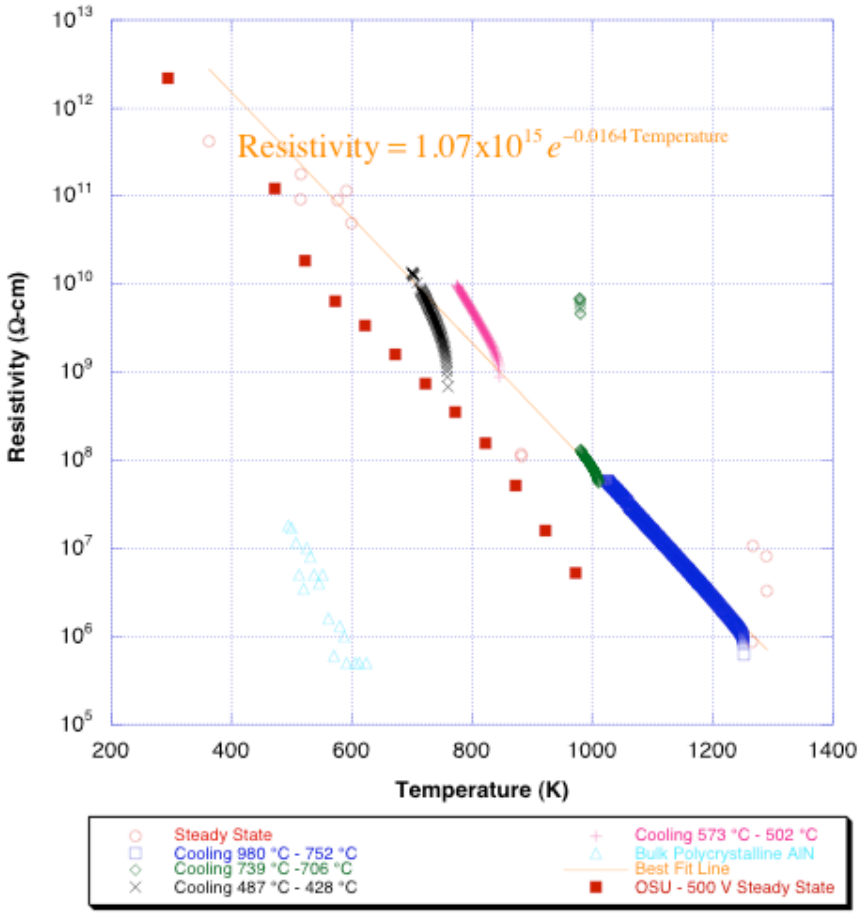

Figure 11—SSFM (381 μm thick) Measured Resistivity Versus Temperature

5.2 Gamma Performance

A wide range of gamma doses delivered by various sources were measured as currents at KAERI: 1) 925 MBq (25m Ci) ^{241}Am, 2) 111 GBq (2 mCi) ^{137}Cs, 3) 111 GBq (2m Ci) ^{60}Co, 4) 6.9 TBq (187 Ci) ^{60}Co, 5) 2.85 PBq (77 kCi) ^{60}Co, and 6) 7.4 PBq (200 kCi) ^{60}Co. Small ^{60}Co sources [18.5 kBq (500 nCi) and 37 kBq (1 µCi)] were used to observe isolated gamma pulses. The lowest total gamma dose rate measured was for the 59.5 keV gamma rays from a 925 MBq (25 mCi) ^{241}Am source located about 3.2 cm from the sensor (approximately 10^7 gamma rays/cm^2-s) with a measured current of 1.8 pA with a leakage current of 0.5 pA. For small source measurements short cables were employed, for the larger sources ~20 m coaxial cables were used. Since no guard conductor was employed (coaxial as opposed to triaxial cables), measurements were also made without the sensor in place and the cable contribution to the measured signal was subtracted manually.

5.2.1 Low Dose Rate Performance

Due to the small size of the SSFMs and the relatively long range of the energetic electrons produced by gamma interactions, the sensors are not in electromagnetic equilibrium. This means that monoenergetic gamma rays do not produce a distinct peak

in a measured pulse height spectrum in addition to limiting the accuracy of the dose deposition estimates. In a fully packaged system, however, the sensor body will be surrounded by alumina or magnesia. Since these are of similar average atomic number and density to the AlN, the devices will be in rough electromagnetic equilibrium in use with roughly as many energetic electrons scattering into the sensor body as out from it.

Gamma induced pulse height spectra were also measured. Either an 18.5 kBq (500 nCi) or a 37 kBq (1 µCi) ^{60}Co source was used to provide the dose. The voltage applied to a 381 µm thick sensor was varied and a pulse height spectrum was measured. A representative pulse height spectrum recorded at 2500 V is shown as Figure 12.

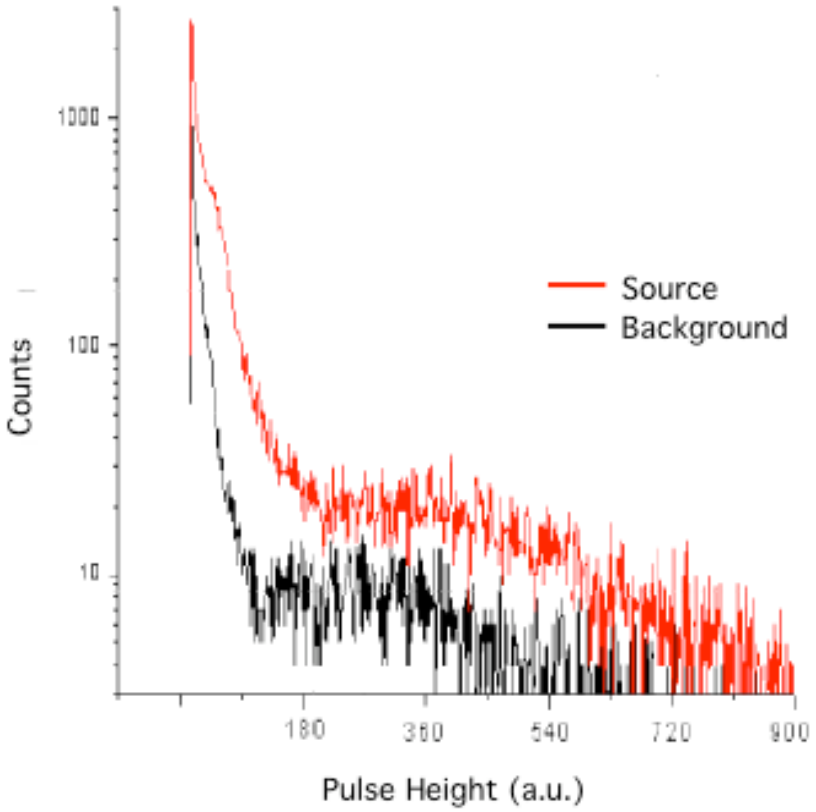

Figure 12—SSFM Gamma Pulse Height Spectrum; 2500 V, 381 μm Thick Detector, 18.5 kBq ^{60}Co Source

The ratio of the number of pulses measured under bias as compared to the number of pulses recorded without a source present was used to determine an optimum operating voltage for a 381 µm thick sensor (see Figure 13).

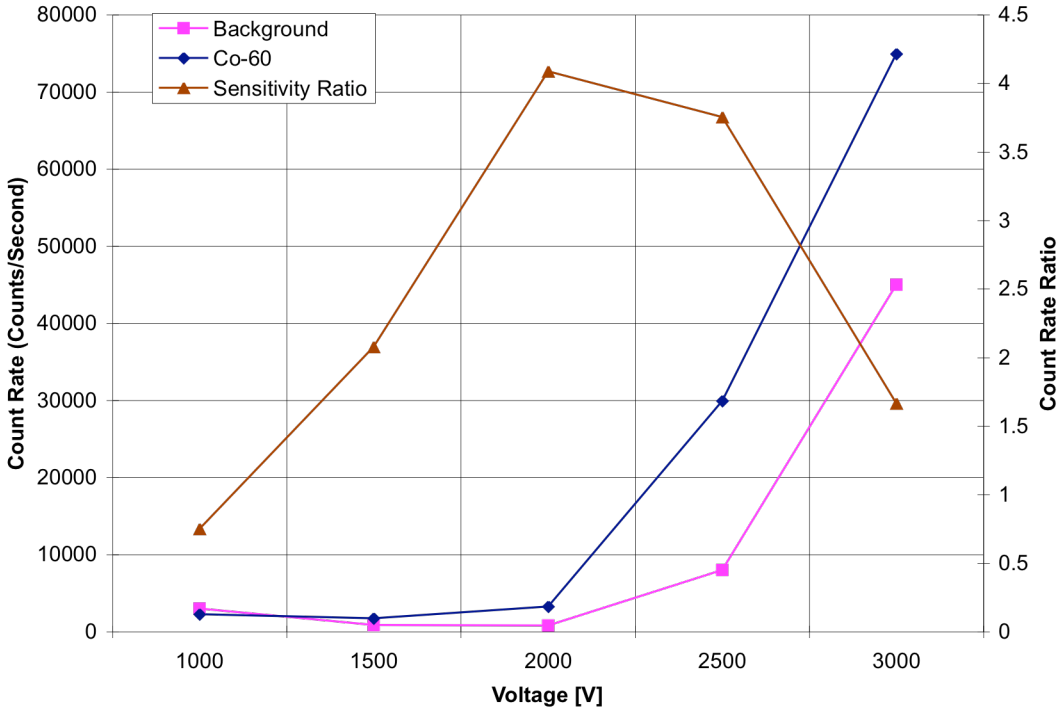

Figure 13—Optimum Operating Voltage Determination - Background and Irradiation Count Rate Versus Voltage

5.2.2 High Dose Rate Performance

High dose rate, gamma induced current measurements of the SSFM were made with two different sources (6.9 TBq ^{60}Co and a 7.4 PBq ^{60}Co) and at three separate distances for each source. The 6.9 TBq ^{60}Co source is a 15 cm long pencil source contained in a pipe of 5 cm diameter. The irradiation set-up is shown in Figure 14.

Figure 14—6.9 TBq ^{60}Co Pencil Source And The Aluminum Nitride Sensor In Holder

The sensor was placed at three different distances from the source and the generated current was measured. The results of the measurements are shown as Table 2. The measured current increases as the applied voltage increases. The response linearity is better when the applied voltage is 500 V or 1,000 V compared with the cases of 1,500 V or 2,000 V.

Table 2—Measurements of 6.9 TBq Co^{60} by a 381 μm Thick SSFM

Distance	Dose Rate [mGy/s]	500V	1,000V	1,500V	2,000V	2,500V
20 cm	13.2	17.5nA	24.5nA	28.4nA	30.8nA	36.7nA
29.3cm	6.53	9.0nA	11.9nA	13.1nA	14.0nA	16.2nA
41.9cm	3.33	4.5nA	5.5nA	6.1nA	6.5nA	7.6nA

A similar set of measurements was performed using the KAERI high gamma dose facility 7.4 PBq ^{60}Co. The measurement results are summarized in Table 3.

Table 3—Measurements of 7.4 PBq ^{60}Co by 381 μm Thick SSFM

Distance from the Source [cm]	Radiation Dose [mGy/s]	Measured Current (SSFM + Cable) [nA]	Net SSFM Current [nA]
160.0	217	280	104
106.4	403	435	162
62.4	861	685	255

The third column of Table 3 shows the measured values at three different distances where the distances are chosen so that the radiation dose rate increases roughly by a factor of two. To determine the fraction of the electric current generated by the electric cable used to apply the high voltage power (1,000 V), measurements with the cable only (i.e., without the sensor) were subtracted from the combined cable and sensor measurements. The results of the two measurement sets are combined and plotted as Figure 15 along with a logarithmically linear fit.

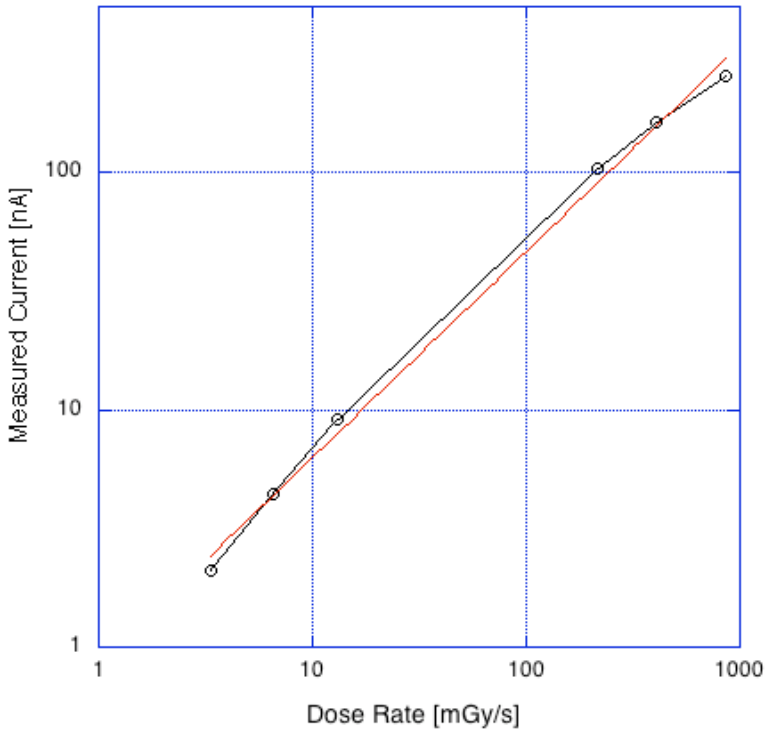

Figure 15—Measured SSFM ^{60}Co Induced Current And A Logarithmically Linear Fit

5.3 Neutron and Mixed Field Performance

5.3.1 Neutron Facilities

Neutron and mixed neutron and gamma field measurements were performed using four facilities: 1) the OSU subcritical assembly, 2) the OSURR, 3) the PNS, and 4) the HANARO (at a beam port (IR port) and within the cold neutron source (CNS) hole).

5.3.1.1 OSU Subcritical Assembly

The OSU graphite moderated subcritical pile, located at the OSURR facility, consists of a 185 GBq (5 Ci) Pu-Be neutron source moderated by nuclear-grade graphite and containing natural uranium fuel rods.[14] The presence of the graphite provides a highly thermal neutron energy distribution away from the source. At the test position, the total neutron flux is approximately 10^4 nv. Figure 22 shows a bare SSFM in a test mount fixture being inserted into a fuel channel of the OSU subcritical assembly.

5.3.1.2 OSURR

The OSURR is a 19.5% enriched U_3Si_2 fueled, light water moderated, pool type research reactor licensed for operation up to 500 kW.[15]

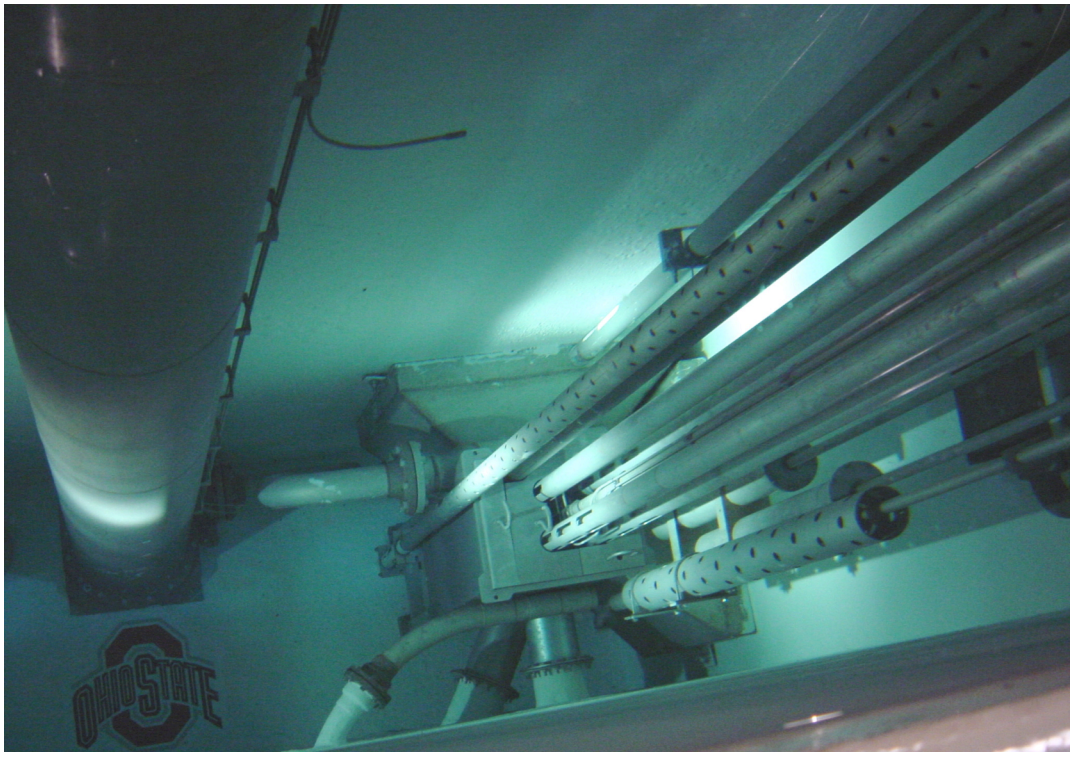

Figure 16—OSURR Core From Pool Top

The OSURR main thermal column consists of 1.524 m long graphite stringers aligned to point away from the core face. The nuclear-grade graphite provides a highly thermalized neutron environment. The position in the graphite lattice denoted as G-5 was selected for the measurements. This position is aligned with the core centerline in the vertical direction, and about 10 cm offset in the horizontal direction from the core centerline. The test assembly was inserted as close as possible to the core face. Figure 17 shows the outer surface of the main graphite thermal column of the OSURR. Position G-5 is located along the horizontal centerline, slightly to the left of the center of the frame. At full operating power, the total neutron flux at the test location is about 1×10^{12} nv, with temperatures at or near ambient.

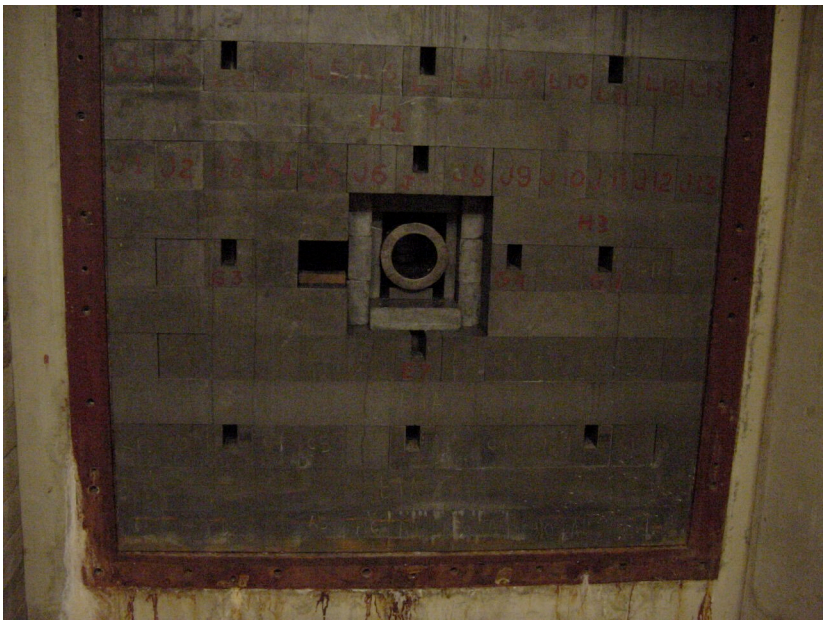

Figure 17—OSURR Main Thermal Column

5.3.1.3 Pohang Accelerator

The PNF is a pulsed neutron facility based on a 100 MeV electron linear accelerator.[16] A cylindrical shell type tungsten target was used for these measurements. The beam parameters used for our experiments were 65 MeV beam energy, 35-50 mA beam current, 1.5 μs pulse width, and10 Hz repetition rate. The total low energy neutron flux, below 10 eV, at our sample location was between 10^8 and 10^9 nv. The neutron to gamma flux ratio of the PNF is more than 100 to 1 (500:1 typical). Figure 18 shows the PNF beam line and a packaged SSFM in location for testing.

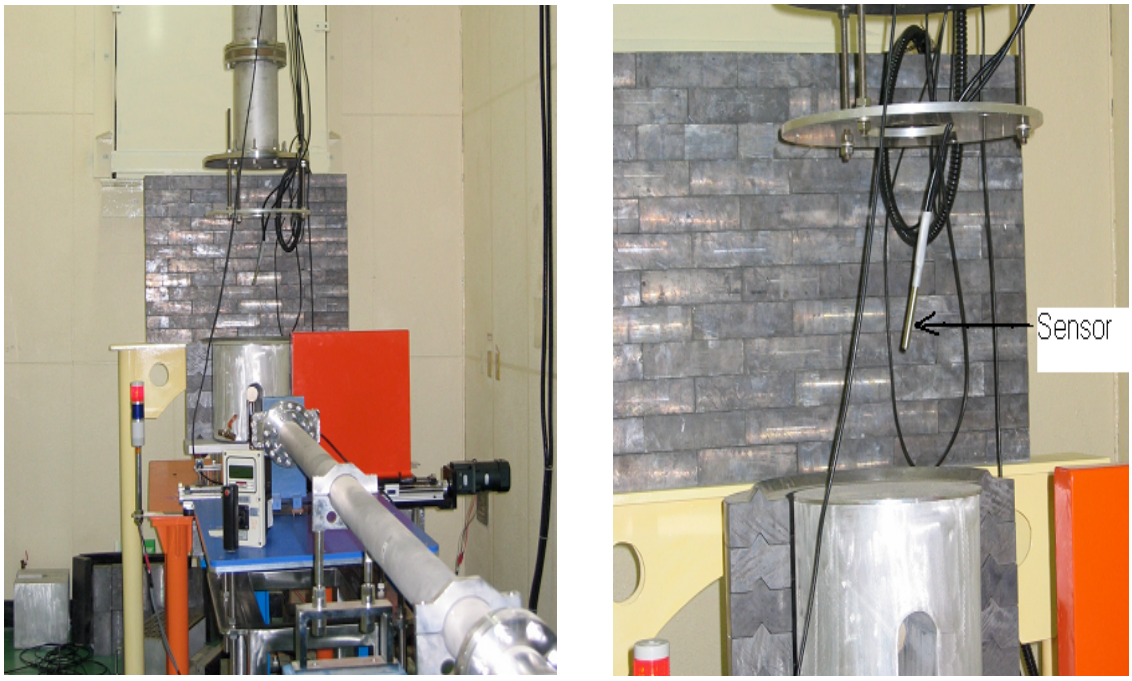

Figure 18—Pohang Accelerator (left) and Sensor Location (right)

5.3.1.4 HANARO

HANARO is a 30 MW_{th} open-tank-in-pool type reactor. It uses light water coolant and heavy water as a reflector. It uses uranium silicide in an aluminum matrix fuel (19.75% enriched) with hafnium absorbers.[17] The IR beam port (see Figure 19) of HANARO was used for the low neutron flux measurements. The thermal neutron flux at the shutter of the IR beam line is ~8 x 10^{11} nv while the fast flux is ~7 x 10^{9} nv. The neutron energy spectrum at the entrance of the IR beam port is well thermalized, but includes the full range of fission neutron energies.

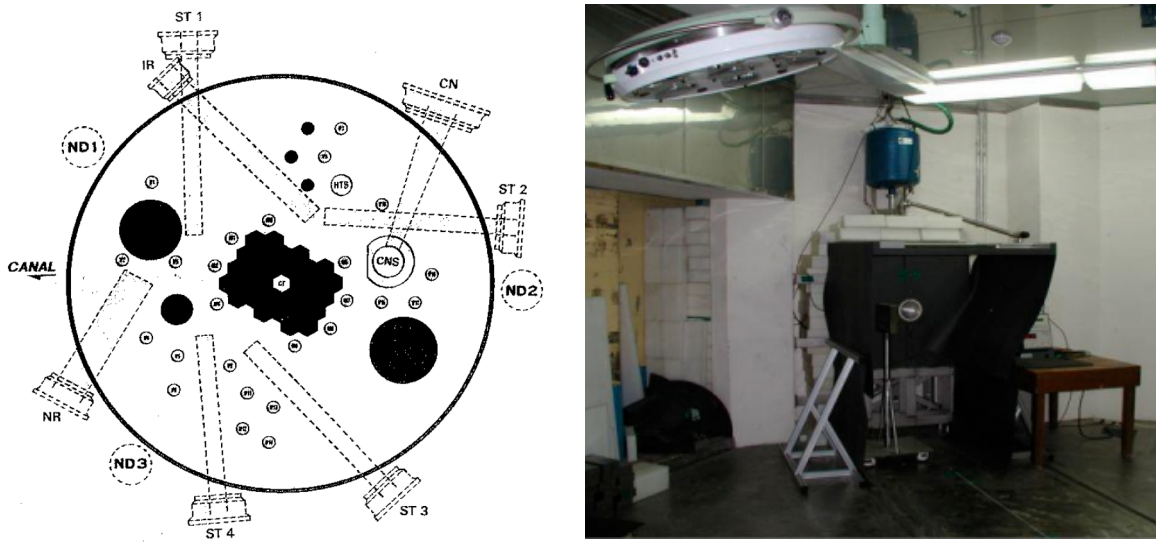

Figure 19—Beam Ports and HANARO; IR Beam Port Used (a) Top View Drawing of Beam Lines and (b) Photograph of IR Beam Port Facility

The HANARO cold neutron source (CNS) hole was used for the high flux measurements,. The neutron flux in the HANARO CNS at full power is 5.72 x 10^{13} nv, and the temperature is ~35 °C. The neutron and gamma spectra in the CNS are shown in Figure 20 and Figure 21 respectively.

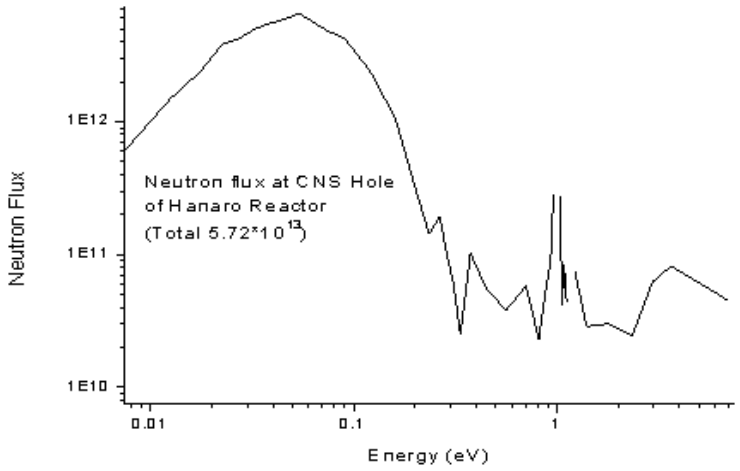

Figure 20—Neutron Flux In HANARO CNS at Full Power

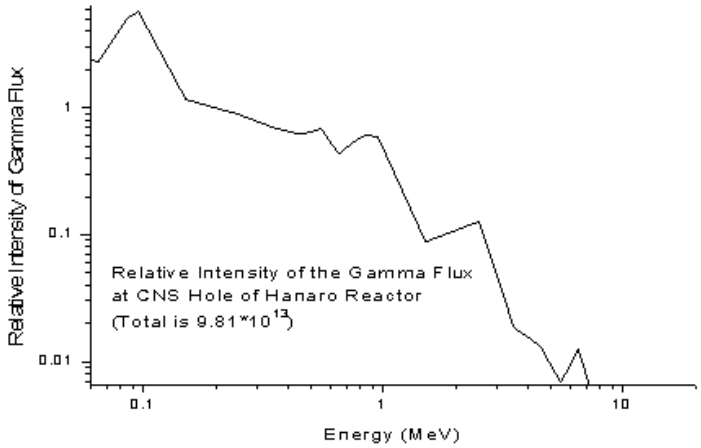

Figure 21—Gamma Flux in HANARO CNS at Full Power

5.3.2 Pulse Measurements (Low Flux)

Neutron pulse measurements were performed using the OSU subcritical assembly, the thermal column of the OSURR, the IR beam port of HANARO, and the PNS. Observing the neutron pulses provides information about the charge motion kinetics within the SSFM. However, the neutron sensitivity of the SSFM is sufficiently low that it is only intended for use in situations where high-absorbed doses are anticipated.

At the OSU subcritical assembly, the SSFM was biased to 1000 V through a Tennelec Model TC-175 charge sensitive preamplifier with a charge conversion gain of 200 mV/pC. The linear amplifier gain was fixed at 500. The detector was connected to the preamplifier via ~5 m of RG-58/U coaxial cable. Note that the sensor itself is exposed, so care was taken to separate the connecting leads during placement into the irradiation position to avoid shorting the leads.

Figure 22 shows the placement of the SSFM and holder assembly into a fuel channel of the subcritical assembly. The holder was positioned at the center of the assembly to attain the maximum neutron flux. Once placed in the neutron flux, the output was observed on the digital oscilloscope. Pulse amplitudes are approximately seven volts. Using the gain of the linear amplifier and the charge conversion gain of the preamplifier, the amount of charge being produced by these measured interactions is about 70 fC. As explained in Section 3.2, a simplistic semiconductor model predicts ~10,000 free carriers (2 fC) to be produced by each neutron capture reaction. It thus appears that the field is sufficiently large within the SSFM to induce some charge multiplication.

In the center of the subcritical pile, the observed pulse rate for neutron interactions was about 0.218 counts per second (cps). Using the estimated thermal neutron flux at the center of the assembly, the sensitivity is thus about 2.2×10^{-5} cps/nv_{th}, corrected for background.

Using the same current measurement set-up as employed in the subcritical assembly studies; initial tests were performed with the sensor located in the OSURR thermal column G5 position with the reactor shutdown but with the reactor start-up source exposed. Based on measured ion chamber data, the flux at the G5 location during shutdown with the start-up source exposed is estimated to be ~1000 nv. The average

SSFM measured pulse rate was 0.02 cps. Using the estimated neutron flux, an SSFM device sensitivity of 2 x 10^{-5} cps/nv_{th} was determined, which quite closely matches the sensitivity determined in the subcritical graphite assembly measurements.

Figure 22—Bare SSFM Being Inserted Into OSU Fuel Channel of OSU Subcritical Assembly

Neutron pulses were measured at the HANARO IR beam port. Figure 23 shows the change in the recorded pulse rate when the beam line shutter was opened. As this is a neutron beam line, most of the recorded pulses likely arise from neutron interactions.

Neutron pulses were also recorded at the PNS using a Inconel™ sheathed sensor. However, the larger cable lengths required at that facility ~30 m required larger fields (increased internal avalanche multiplication) to obtain measurable pulses; 3000 V applied across a 635 μm thick sensor.

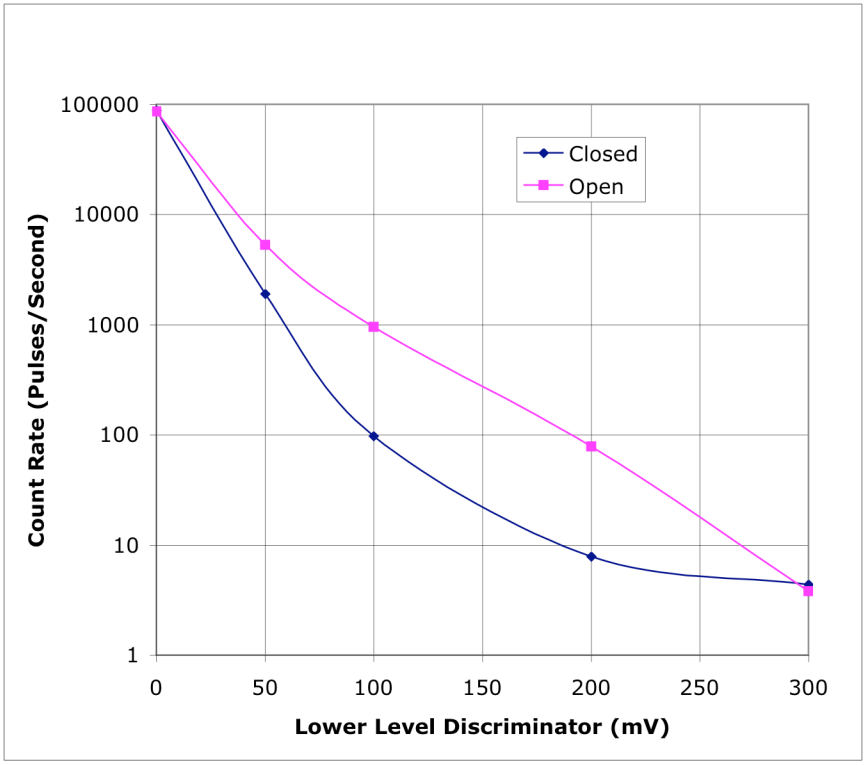

Figure 23—Measured Detector Pulse Rate Change When Opening HANARO IR Beam Line Shutter

5.3.3 Current Measurements (High Flux)

Current measurements were performed under high dose conditions at the OSURR, the PNS, and at HANARO.

5.3.3.1 OSURR

Initial testing of the prototype SSFM in current mode operation was conducted at position G-5 in the main thermal column of the OSURR. At full operating power, the total neutron flux at the test location is ~10^{12} nv, with temperatures at or near ambient. In this test, the reactor power was first increased to full power, then reduced in increments for check linearity of device response, followed by a return to full power and a test of response to a sudden drop in power (scram). The power increments for the OSURR are 450 KW (indicated nuclear power), 250 KW, 100 KW, 50 KW, and 10 KW. The rod insertion time for the scram response is about 350 milliseconds.

Figure 24 shows the measured sensor current. The power increments can be observed as well as the initial "ramp" increase in power, and the scram shutdown, which ended the operation. Subsequent power decay following the scram can be observed in the sensor output. The dynamic range of the sensor indicates that it would perform reasonably well as a power range monitor. The sensitivity of the SSFM operated under these conditions is about 7.9 x 10^{-20} A/nv, similar to some versions of hafnium-based SPNDs.

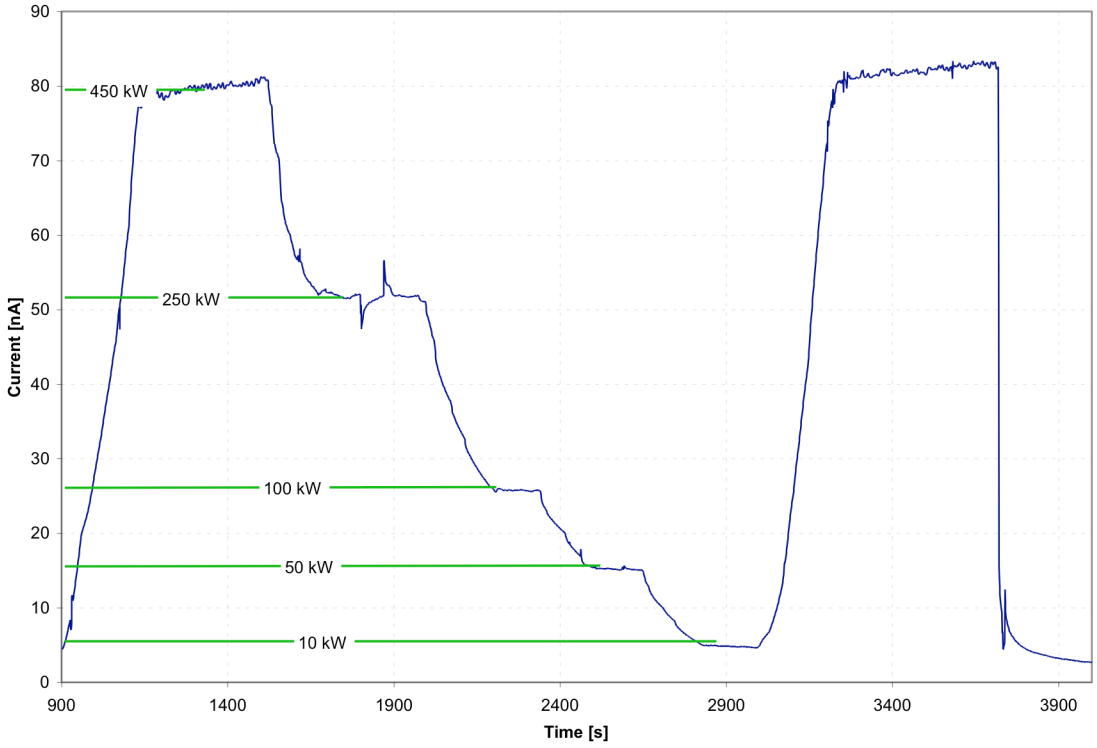

Figure 24—Measured SSFM Current in G-5 Location of the Thermal Column of OSURR As Reactor Power is Changed

The sealed SSFM unit supplied by Woojin Inc. was tested for transient response to a reactor scram from full power. This response was compared to that of a conventional compensated ion chamber (CIC), which is a normal part of the OSURR reactor control system.

The OSURR was operated at full power for several minutes before the initiation of the scram. At the time of the scram, all three shim safety rods were fully inserted to drive the reactor power to shutdown levels as quickly as possible. The detector was placed in the OSURR Central Irradiation Facility (CIF) to assure that the maximum possible flux was incident upon the SSFM. Under these conditions, the OSURR thermal power is 450 KW, and the total neutron flux incident upon the SSFM before the scram was about 2.3×10^{13} nv. The total time for control rod insertion is about 300 milliseconds.

The detector outputs were recorded using a computer-based data acquisition system. The data capture rate was one second per sample. The computer provides a time stamp for recorded data so data capture channels can be aligned in time. Once recorded, the detector outputs were normalized to their maximum value during the data capture to allow comparison of the dynamic response of the sensors.

Figure 25 shows the results of this test. The SSFM tracks the CIC response for the initial portion of the transient, with a slightly slower response time. As the power drops to the shutdown range, the SSFM shows a higher normalized output. This likely indicates that the SSFM output includes a significant gamma component following shutdown compared to that of the CIC. This is not unexpected as the CIC includes electrical subtraction of the

gamma component of the signal. The SSFM, at this point in its development, does not have this feature. In spite of this, the SSFM provides a reasonably valid and predictable response to a sudden drop in incident flux.

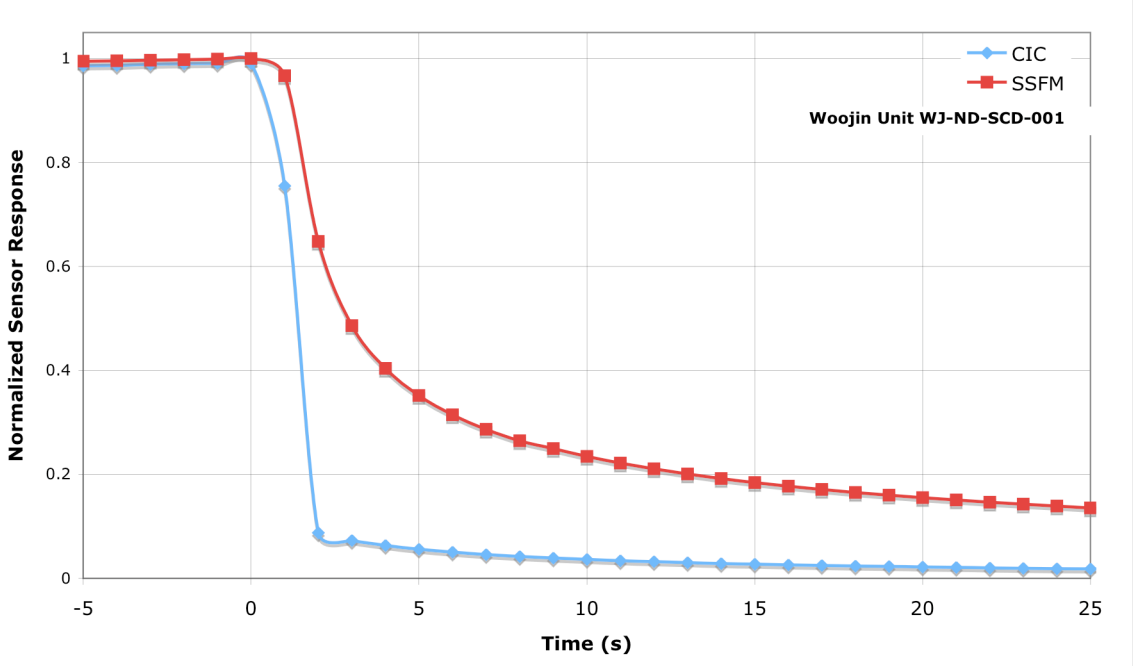

Figure 25—SSFM SCRAM Response Compared to CIC

The temperature of the same sealed SSFM unit supplied by Woojin was recorded to observe any correlation between the SSFM measured current and its temperature. While the non-nuclear resistivity versus temperature testing (see Figure 11) indicates that below 475 °C minimal change in the measured detector current is anticipated with changing temperature, it is possible that radiation may change the dynamics of the device polarization. As with the scram response, the SSFM output was compared to that of the OSURR reactor control system CIC.

The OSURR was operated at full power for several minutes to observe the stability of the SSFM output signal as the detector experienced heating by radiation absorption. A Type-K thermocouple was placed in contact with the sensor body to provide an indication of sensor temperature. As with the scram response tests, the detector was placed in the CIF to deliver the maximum possible flux to the SSFM. This provided the highest signal magnitude as well as inducing the maximum heating.

The CIC, SSFM, and thermocouple detector outputs were captured at one-second intervals for several minutes. Figure 26 shows the results of this test. The SSFM output drifts upward over time resulting in an artifact in the measured current. The apparent reactor power trends upward as measured by the SSFM, although the CIC shows the true power to be steady. The increase in the SSFM measured current ceases at roughly the same time that the temperature rise stops. It remains unclear whether the SSFM is responding to its internal temperature rise or another time or external temperature dependent phenomenon such as increased leakage current in the device packaging with

increased temperature. It is recommended to pursue further testing employing non-nuclear heating of packaged and unpackaged devices to isolate the cause of the drift.

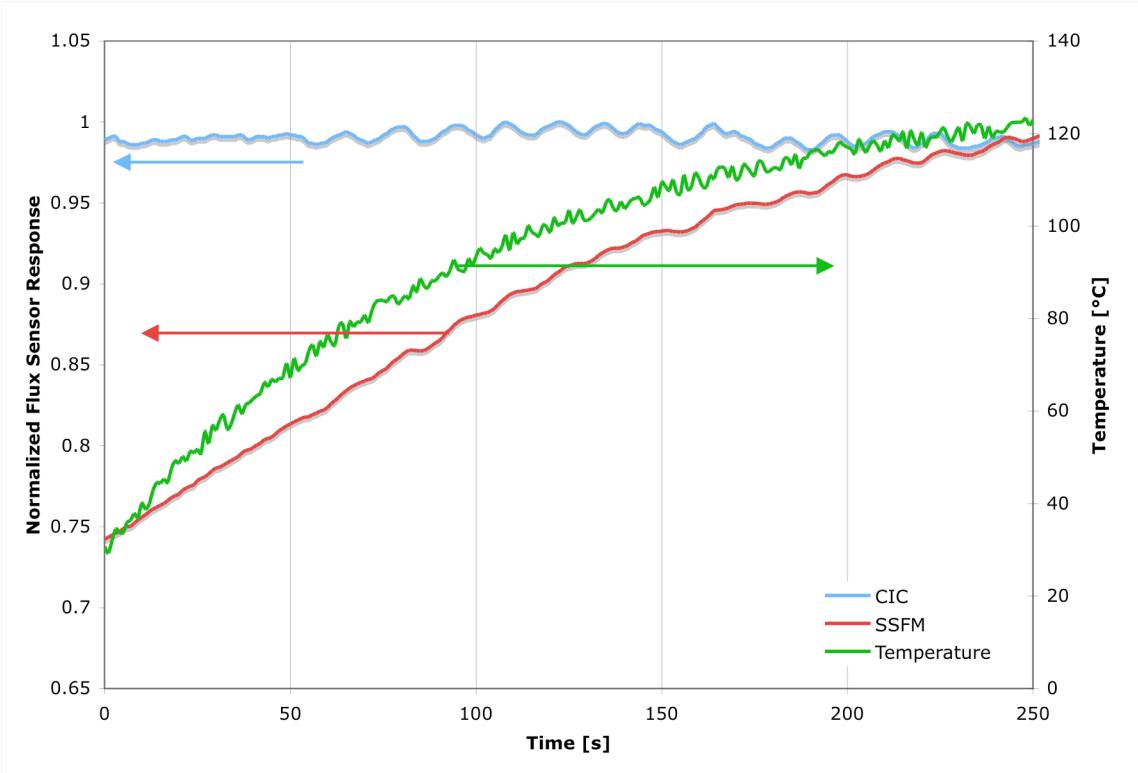

Figure 26—CIC and SSFM Response Changes & SSFM Temperature Change

5.3.3.2 PNS

A series of SSFM current measurements were made at the PNS. For these measurements, the a 635 µm thick SSFM was biased to 3000 V and connected to an electrometer across 30 m of signal cable. Note that this is the same sensor in the same conditions as for the lower flux measurements at PNS. A plot of the measured SSFM currents is shown as Figure 27. The bottom curve Figure 27 shows the background curve taken before the power of the accelerator was turned on. The second curve from the bottom is taken with the sensor furthest from the beam target (neutron source). The top curve shows the measured values when the sensor is located nearest to the target. Much of the recorded fluctuation in the measured current is due to fluctuations in the electron beam current, which varies fractionally roughly the same amount with the same time characteristics.

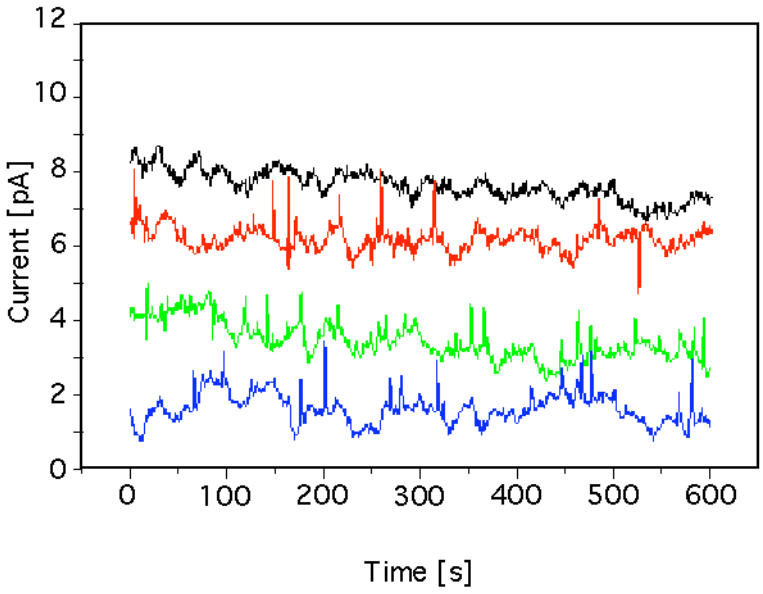

Figure 27—Measured SSFM Current At Different Distances From Target at PNS; Bottom Curve Background

The detector response was tracked while the accelerator power was cycled repeatedly to determine the time response characteristics of the sensors. Note that the background noise is about 7pA when the applied voltage to the detector was 3,000V. Figure 28 shows how the measured current increases when the electron beam power was turned on initially. The sensor reaches its maximum response (15 pA) in about 22 minutes. The electron beam bower was then cycled off and on for three-minute intervals. Figure 29 is an enlarged graph of the current during the time period of the on-off operation.

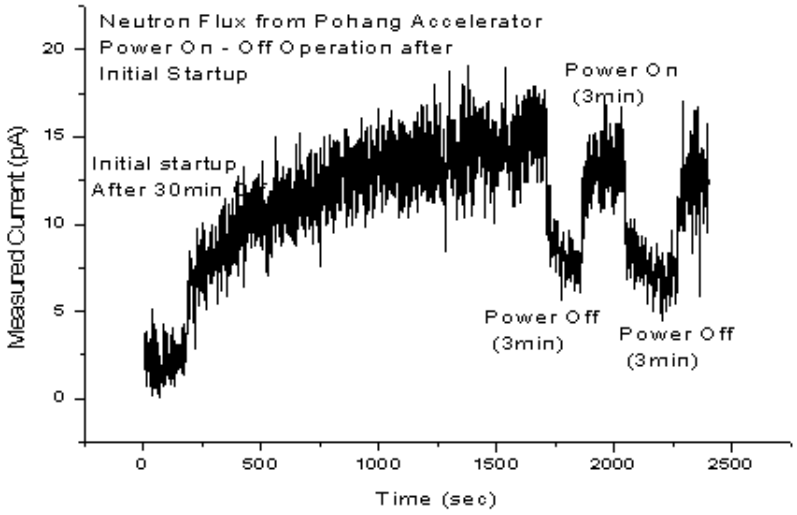

Figure 28—Time Response of SSFM at PNS To Beam Switching On and Off

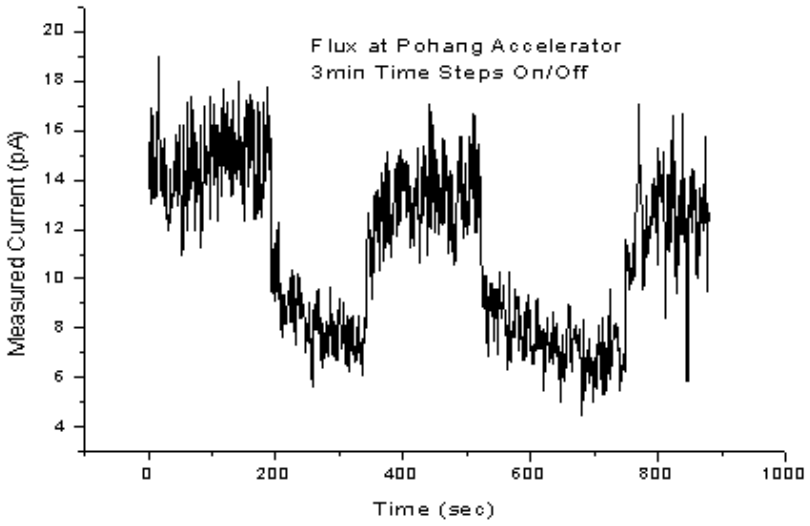

Figure 29—Measured Current At PNS During As Electron Beam Cycles On and Off

5.3.3.3 HANARO

A packaged SSFM 381 μm thick was deployed in the HANARO CNS and its generated current was recorded as the reactor maneuvered in power. The SSFM was packaged in a capsule as described earlier (see Figure 6) with a pair of 16 m long mineral insulated signal cable attached and inserted into an aluminum guide pipe and sleeve. The deployed sensor resistance, including cable leakage, was greater than 5 TΩ.

The detector current was measured while the reactor power is being increased from 1 MW to 8M W, held steady at 8 MW for an hour, increased from 8 MW to 13 MW, and finally the reactor was tripped. The measurement results are shown as Figure 30. The current produced by the SSFM varied linearly with the reactor power over the reactor power range used (0% to 43% full power).

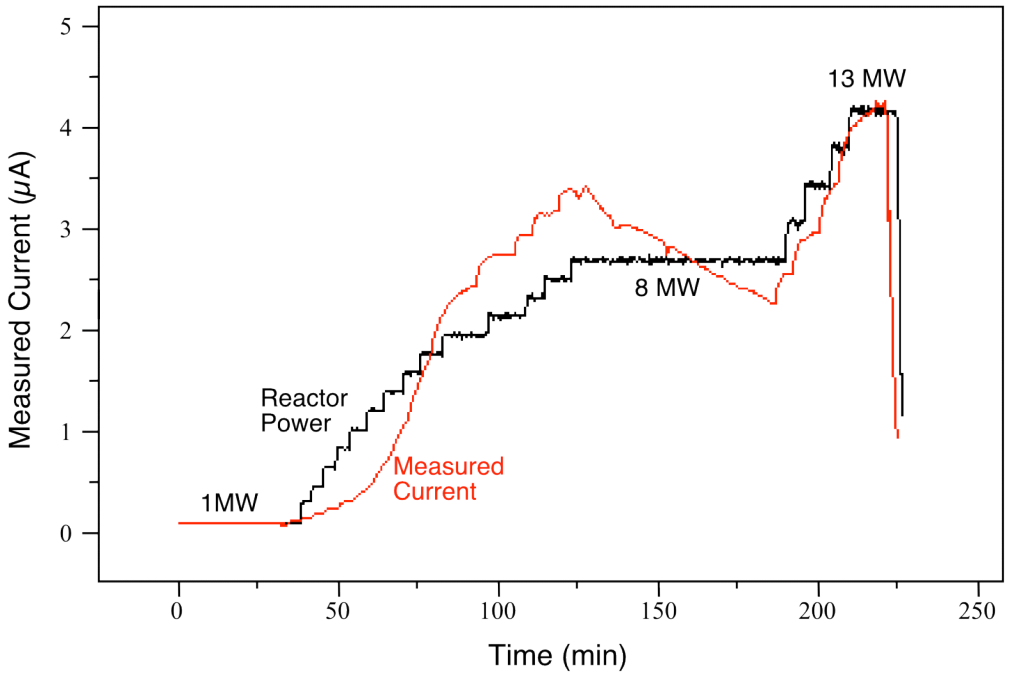

Figure 30—Correspondence of SSFM Current Measurement With HANARO Power

The reason for the delayed increase in the measured current as the reactor begins to ascend in power may be the low voltage applied to the detector. The devices respond more rapidly when higher voltages (3000 V) are applied to them. However, only 1000 V could be applied using the cabling available in the reactor. It is speculated that the decrease in the measured current while the reactor power held constant at 8 MW may reflect device polarization; impurity ions inside the detector body migrate under the applied field and form a dead region whose size increases with time.

6 Conclusions

A novel solid-state sensor for measuring dose and neutron flux in-core, at power in nuclear reactors was conceived, designed, fabricated, and tested for this project. The basic performance characteristics of the sensor have been established. The transducer essentially consists of an AlN sintered compact with DBC contact pads and ultrasonically bonded copper lead connections. This is the first known use of a solid-state resistive type device as a flux/dose monitor under in-core nuclear reactor type environments. The measured device performance parameters are similar to those expected theoretically. The SSFM functions as both a neutron pulse monitor and a dose sensitive resistive element.

Further development is required before these devices can be considered for deployment into nuclear power plants. The stability of the device requires considerable further investigation as device polarization appears to be significant at the current development level. Also, an improved high temperature design, reducing the leakage current, is required to implement the device at core temperatures above those of water reactors. Further, the long-term survival of the devices under in-core environments remains unknown. Transmutation doping of the AlN with the ^{14}C resulting from the neutron

capture requires particular attention. In general, device repeatability and consistency needs to be further investigated as this project has not thoroughly evaluated the myriad possible device and cabling configuration variations. Finally, gamma compensation, substituting ^{15}N (lacking the neutron capture cross section) for ^{14}N in the sensor body should be demonstrated. This would establish a purely neutron flux measurement technique analogous to a compensated ion chamber.

---

[1] K. P. Ananthanarayanan, P. J. Gielisse, and A. Choudry, *Boron Compounds for Thermal-Neutron Detection*, Nuclear Instruments and Methods, 118 (1974), 45-48

[2] http://www.ill.fr/News/34/34_news7.htm

[3] K.R. Prasad, S.P. Chaganty, V. Balagi, E. Unnikrishnan, K. Venkateswara Rao, "Development and Applications of LPRM Detectors," *Nuclear Instruments and Methods in Physics Research A*, **418**, 1998, pp. 420-8

[4] M.F. Ohmes, D.S. McGregor, J.K. Shultis, P.M. Whaley, A.S.M. Sabbir Ahmed, C.C. Bolinger, T.C. Pinsent, "Development of Micro-Pocket Fission Detectors (MPFD) for Near-Core and In-Core Neutron Flux Monitoring," *Proc. SPIE*, Vol. 5198 (2003) pp. 234-242.

[5] S. Seshadri, Abdul R. Dulloo, Frank H. Ruddy, John G. Seidel, and L.B. Rowland, "Demonstration of an SiC Neutron Detector of High-Radiation Environments," *IEEE Transactions on Electron Devices*, **46**(3), March 1999, pp. 567-72

[6] Frank H. Ruddy, Abdul R. Dulloo, and John G. Seidel, "Silicon Carbide Semiconductor Neutron Detectors," *Fourth American Nuclear Society Topical Meeting on Nuclear Plant Instrumentation, Controls, and Human-Machine Interface Technologies (NPIC&HMIT 2004)*, Columbus, Ohio, September 2004

[7] Properties of the Group III Nitrides, James H. Edgar editor, INSPEC, London, 1994, ISBN 0852968183

[8] http://www.ioffe.rssi.ru/SVA/NSM/Semicond/index.html

[9] http://www.valleydesign.com

[10] http://www.curamik.com

[11] W.B. Carter and M. V. Papageorge, *Titanium and tantalum coatings on aluminum nitride*, Journal of Vacuum Science and Technology A, Vol 10(6), Nov/Dec 1992, pp. 3460-4

[12] M. Entezerian and R.A.L. Drew, *Direct Bonding* of *Copper to Aluminum Nitride*, Materials Science and Engineering, A212 (1996), 206-212

[13] M. Bickermann, B. M. Epelbaum and A. Winnacker, *Characterization Of Bulk Aln With Low Oxygen Content*, Journal of Crystal Growth, **269**(2-4), 1 Sep. 2004, pp. 432-42

[14] http://www-nrl.eng.ohio-state.edu/facilities/subcrit.html

[15] http://www-nrl.eng.ohio-state.edu/facilities/reactor.html

[16] G.N. Kim, Y.S. Lee, D. Son, H. S. Kang, M. H. Cho, I. S. Ko, and W. Namkung, *Photoneutron Spectrum At Pohang Neutron Facility Based On 100-Mev Electron Linac*, Proceedings of the 2001 Particle Accelerator Conference, Chicago, Illinois, June 18-22, 2001, pp 2542-5 (http://epaper.kek.jp/p01/PAPERS/WPPH043.PDF)

[17] http://hanaro.kaeri.re.kr/